Pronounced effects of oxygen growth pressure on structure and properties of ZnO and AZO films laser deposited on Zeonor polymer

*Saikumar Inguva, Enda McGlynn, Jean-Paul Mosnier**

School of Physical Sciences and National Centre for Plasma Science and Technology,

Dublin City University, Glasnevin, Dublin 9, Ireland.

* Corresponding author:

Email addresses: Jean-Paul.Mosnier@dcu.ie

Tel: +353 1 700 5303

Key words: *ZnO and AZO, thin films, pulsed-laser deposition, oxygen growth pressure, room temperature deposition, Zeonor polymer, flexible substrates, flexible optoelectronics*

Abstract

We report the pronounced effects of oxygen growth pressure (0.13 Pa-40 Pa) on the surface morphology, hydrophobicity, structural, optical and electrical properties of ZnO and aluminium-doped ZnO (AZO) thin films deposited by room temperature pulsed-laser deposition on the low water-absorbing polymer Zeonor. Significant changes were observed for oxygen growth pressures below ~ 10 Pa. In this pressure range, the morphology changed from nanocrystalline to that of a continuous film with a shift of the growth orientation of the crystalline fraction of the deposit from *c*-plane to *m*-plane. The appearance of valley-shaped surface cracks caused a significant increase of rms surface roughness, reduced hydrophobicity and shift to hydrophilicity at 0.13 Pa. The visible optical transmittance of the film reduced from an average of 90 % to 65 % and the orange/red deep level emission was quenched. The electrical properties showed decreasing resistivities (10^5 Ω cm to 10^{-3} Ω cm) and Hall mobilities (35 cm^2/V-s to 3 cm^2/V-s) and increasing carrier concentrations (10^{11} cm^{-3} to 10^{21} cm^{-3}). These significant changes of the films physical characteristics were related to the morphological and structural changes induced by the change of oxygen growth pressure. The observed effects are interesting for applications in flexible optoelectronics and briefly discussed in this context.

1. Introduction

Further advances in the field of flexible optoelectronics [1,2] require detailed understanding of the deposition and growth processes leading to high-quality thin films of transparent conductive oxide (TCO) materials on flexible substrates [3-8]. This is key to achieving controllability of both structure (amorphous versus crystalline) and fundamental semiconductor properties such as carrier concentration [9] or work function [10]. In this regard, high-quality, indium-free, ZnO, AZO (ZnO:Al) and other ZnO-based oxide films, have been successfully deposited on sundry plastic/polymer substrates for specific applications. We give recent and relevant examples of such works.

In the field of sustainable energy, 100 nm thick (001)-oriented ZnO electrodes were deposited on PET substrates by RF sputtering for water splitting applications [11], while densely packed *c*-axis oriented ZnO nanogenerators were grown on flexible polyester substrates using wet chemical methods [12]. Polycrystalline ZnO thin film transistors (TFT) were successfully produced on polyimide (PI) and polytethylene theraphtalate (PET) substrates using cathodic arc deposition at room temperature (RT) [13] and atomic layer deposition (ALD) at around 100 ˚C [14,15], respectively. In the field of organic light emitting diodes (OLED), (002)-textured AZO electrodes have been deposited on PET using plasma-sputtering at RT [16] while ALD was used to deposit a ZnO film, acting both as a gas-diffusion barrier and an electron-injection layer, in a plastic-based, encapsulated, hybrid-OLED device [17]. AZO has been used extensively in works on flexible solar cells and deposited on PET both by RF magnetron sputtering at 100 ˚C [18] and pulsed-laser deposition (PLD) at RT [19]. The latter technique was also used to deposit zinc indium tin oxide (ZITO) amorphous transparent electrodes in ultraflexible polymer solar cells [20] and nanostrutured ZnO was deposited by chemical bath deposition (CBD) at RT on PET substrates for flexible dye-sensitized solar cells [21]. In biological applications (e.g. antibacterial materials, biosensing), ZnO thin films and

77 nanostructures were deposited on flexible bi-axially oriented polypropylene and textile carbon
78 substrates by ALD at around 100 ˚C [22] and an aqueous chemical growth method at 90 ˚C
79 [23], respectively.

80 In parallel with these application-driven works, a considerable research effort is also
81 being devoted to the development of novel deposition methods of ZnO and ZnO based-
82 materials on flexible plastics and the study of the corresponding thin film material properties.
83 These include roll-to-roll RT sputtering [24], RT plasma sputtering on bent substrates [25],
84 PLD at RT [19,26], sol-gel spin coating [27], direct writing [28], low temperature ALD [29],
85 atmospheric plasma deposition [30], seeded-growth with CBD [31] and RF magnetron
86 sputtering at RT [32]. In addition to the properties of the active oxide layers, those of the
87 flexible substrate are equally important for the optimization of a given application (see details
88 in ref. [33]).

89 This brief review of selected works has highlighted the wide range of structures (from
90 amorphous to single-crystalline) and morphologies (from thin films to nanostructures) of ZnO
91 material that is needed to achieve the required physical/chemical characteristics of working
92 devices in an equally wide range of applications. A common and key requirement for work on
93 flexible plastics is the availability of deposition methods optimised for high-quality oxide
94 layers at RT or low temperature (~ 100 ˚C). However, a significant drawback in flexible
95 optoelectronics is due to gas, notably oxygen, and water vapor diffusion which can have
96 deleterious effects and significantly shorten the active layers' quality lifetime and, thus, device
97 overall reliability [34,35]. Ceramic layers are recommended as gas barrier layers [36] and thin
98 film ZnO on polyethylene naphthalate (PEN) was recently used in a hybrid-OLED device with
99 the dual purpose of acting simultaneously as an electron-injection and gas-barrier layer, as
100 mentioned earlier [17].

In this work, we investigate the material properties of ZnO and AZO films, deposited by pulsed-laser at RT on Zeonor which is a brand of cyclo olefin polymer (COP) flexible plastic. Zeonor has unique, advantageous and superior material properties compared to other plastic materials [37-39], including significantly lower water absorption (< 0.01 %), high optical transmission (> 90 %) and larger hydrophobicity. The work notably shows the significant effect of the oxygen deposition pressure on the structural and electrical properties of the oxide layer material, featuring transitions of the films' morphological/electrical properties from continuous/conductive to nanostructured/semi-insulating with increasing oxygen deposition pressure.

2. Experimental Details

The films were grown in a commercial PLD apparatus (Neocera Pioneer 180 UHV module) with substrate load-lock, automated process pressure control and additional hardware and software capabilities for continuous composition spread over a 2" diameter disk. The samples were nominally at RT. The PLD apparatus is equipped with a high-power, Q-switched, frequency-quadrupled Nd:YAG laser. The wavelength output, repetition rate, pulse width, and energy of the laser pulse were 266 nm, 10 Hz, 6 ns, and 150 mJ, respectively. An average laser fluence on the target used was about 2.0 J/cm^2. The distance between target and substrate was kept constant at 5 cm. A ZnO target (99.99 % pure) and an AZO target (2 wt % Al_2O_3) were used. Sheets of 1.2 mm thick 1060R Zeonor cut into 1 cm × 2 cm rectangles were used as substrates. Before loading the Zeonor substrates into the PLD chamber, the substrates were gently cleaned with isopropyl alcohol and then dried with nitrogen gas. Base pressure of the PLD chamber was kept constant at around 3.9×10^{-6} Pa for all the growths. Growths were carried out in ambient oxygen pressures, with high purity (99.999%) oxygen gas, ranging from 0.13 Pa (1 mTorr) to 40 Pa (300 mTorr), maintained constant by adjusting the turbomolecular

pumping speed at a constant oxygen flow rate of 100 sccm. Growth parameters and sample details are given in Table 1. In all cases, the properties of the as-grown films were measured.

Film thicknesses and surface morphologies were measured using a Dektak profilometer (D150 Veeco) and an atomic force microscope (AFM) in tapping mode (Dimension 3100 controlled by Nanoscope IIIa controller, Digital Instruments), respectively. The water contact angle (WCA) was measured by the sessile drop technique with high purity HPLC grade water, using a computer-controlled instrument (contact angle analyzer FTA200, USA). The structural characteristics were investigated by 2θ-ω x-ray diffraction (XRD) scans (Bruker AXS D8 Advance Diffractometer) using the Cu K_{α} characteristic emission of wavelength 0.15418 nm. Optical transmittance were measured using a UV-visible double-beam spectrophotometer with millimeter beam spot size dimension at the probing location (Varian CARY 50 scan). Measurements of electrical properties were carried out using a commercial 4-point probe/Hall effect apparatus (Accent HL5500). No extra contacts were deposited and/or soldered on the samples for these measurements. The system four probes were placed directly onto the sample surface in the Van Der Pauw configuration always forming ohmic contacts as checked by the acquisition software. The Hall effect measurements were all performed at the system fixed magnetic field intensity of 0.51 T under the prevalent conditions of pressure and temperature.

The statistical or experimental errors associated with all the above measurements are recorded, where possible, as error bars on the relevant graphs.

3. Results and discussions

3.1 Surface properties

Fig.1 shows AFM images of selected samples. For pressures of 10 Pa (75 mTorr) and above, the deposited films present similar microstructures, typically granular (nanocrystalline) with lateral grain sizes of 75 nm - 200 nm. This is a commonly observed microstructure for

ZnO, characteristic of the so-called high-pressure growth regime, attributed to gas-phase collisions between the ablation plume and the oxygen background gas [26,40]. At oxygen pressures of 10 Pa (75 mTorr) and below, significant morphological changes are observed in both the ZnO and AZO films: The deposits present continuous, film-like, morphologies. Additionally, the pattern of shallow (10 nm) hairline cracks, observed in the middle panels of Fig.1, evolves into deep (150 nm) and narrow valleys for the samples grown in 0.13 Pa (1 mTorr) oxygen pressure.

The root-mean square (rms) surface roughness (R_q) of each film was estimated over an area of ~ 5 μm x 5 μm (512 pixels × 512 pixels) from the AFM data, using the WSXM image processing software, and is shown as a function of oxygen pressure in Figure 2. The rms roughness of the bare Zeonor was measured around 0.5 nm. As the oxygen pressure decreases from 10 Pa (75 mTorr) to (0.13 Pa) 1 mTorr, R_q increases significantly from 5 nm to 65 nm for both the ZnO and AZO films. This can be related to the patterns of striations and valleys mentioned above. The depth (~ 150 nm for the 0.13 Pa (1 mTorr) samples) of these features significantly influences the value of R_q as expected. Indeed, the rms (R_q) and average (R_a) roughness determined over 1 μm x 1 μm areas free from these features decreases to 23 nm and 18 nm, respectively. The variations of WCA with oxygen pressure are shown in the inset of Fig 2. The WCA of 92° for the bare hydrophobic substrate 1060 R Zeonor is slightly hydrophobic. As the oxygen pressure decreases, the WCA values decrease from 111° to 88° and from 92° to 80° for ZnO and AZO, respectively. Thus, the degree of hydrophobicity decreases with oxygen pressure. Only the samples grown at 0.13 Pa (1 mTorr) oxygen pressure show a clear hydrophilic behavior. Wetting properties depend on the surface texture, roughness and crystal structure [41,42]. The observed decrease of hydrophobicity with oxygen pressure is consistent with both the observed surface roughness increase and the surface texture and grain size decrease (see XRD data below) with decreasing oxygen pressure. The relationship

of hydrophobicity to the surface texture can be explained in terms of trapped air volumes on the film surface: A large number of air traps increases the hydrophobic behavior [42]. This is consistent with the present work because the number of air traps is likely to be greater for the films with nanostructured grains formed at oxygen pressures ≥ 3.33 Pa (25 mTorr).

3.2 Structural properties

Fig. 3 shows 2θ-ω XRD scans for ZnO and AZO films grown at different oxygen pressures by room temperature PLD on Zeonor plastic substrates. The ZnO films grown at oxygen pressures above 0.13 Pa (1 mTorr) show dominant (002) and (004) peaks indicative of the wurtzite structure with *c*-plane orientation. The ZnO film deposited at 0.13 Pa (1 mTorr) shows the (100) peak dominant, indicative of a change from *c*-plane to *m*-plane orientation of the crystalline fraction. The reduction in overall signal intensity may indicate an increased amorphous deposit fraction for the samples grown at the lower oxygen pressures. The AZO films grown at oxygen pressures above 1.33 Pa (10 mTorr) also show dominant (002) and (004) peaks, whereas those grown at oxygen pressures below 3.33 Pa (25 mTorr) show a complete absence of the (002) peak and the growth of the (100) peak. Again, the reduction in overall signal intensity may indicate an increased amorphous deposit fraction for the samples grown at the lower oxygen pressures. Previous works have also shown an amorphous structure for AZO and IZO films grown by room temperature PLD on PET substrates, for example ref. [43]. The observed shift of crystalline fraction orientation correlates with the previously discussed shift from nanocrystalline to continuous film-like morphologies in the same oxygen pressure domain.

In order to study the effect of oxygen pressure on crystalline quality, we have measured the (002) peaks 2θ angular position and FWHM values. The results are listed in Table 1. For reference, we have also measured a *c*-axis oriented ZnO single crystal wafer of thickness 0.5

mm (Tokyo Denpa) with the same apparatus: the corresponding 2θ and *c*-parameter values are 34.45º and 0.5207 nm, respectively. It is seen that for oxygen pressures above 3.33 Pa (25 mTorr) the 2θ angular value decreases and diverges from the ZnO bulk value as oxygen pressure decreases for both ZnO and AZO films. However, for the oxygen pressures of 3.33 Pa (25 mTorr) and 1.33 Pa (10 mTorr), this trend does not hold and the 2θ angular value increases towards the bulk ZnO value for both ZnO and AZO films. This relaxation towards the bulk crystal value is consistent with the presence of hairline cracks and deep valleys discussed previously. In most of the cases the 2θ angular values are smaller than the ZnO wafer value. We have estimated the *c*-axis lattice parameter (from Bragg's law) and the residual stress in the ZnO and AZO films plane using the bi-axial strain model developed in ref. [44] (see also ref. [26] for experimental details). This approach assumes that stress is quite uniform over large distances and, thus, macrostress prevails. This is a reasonable assumption for highly textured films [45]. The values are shown in Table 1. In all cases (except AZO grown at 40 Pa (300 mTorr)), the films are tensilely strained normal to the substrate and thus subject to compressive strain in the substrate plane. From the experimental full width at half-maximum (FWHM) of the (002) peaks, we have evaluated average crystallite sizes using Scherrer equation with a particle shape factor of 0.9 [45,46]. The 0.167° (002) peak FWHM for the ZnO wafer was taken as the instrumental width and removed assuming Gaussian broadening. The results are shown in Table 1. As oxygen pressure increases, the (002) FWHM decreases, which can be taken to represent a proxy measure of crystalline quality. The average crystallite sizes are in the range 2-21 nm and 3-18 nm for the ZnO and AZO films, respectively, and comparable with previously reported values for ZnO/AZO thin films deposited on amorphous substrates [46,47]. It is notable that significant increases in the crystallite size occur at the oxygen pressure values where film morphological changes are also observed (see above discussions).

3.3 Optical properties

Fig. 4 shows the optical transmission spectra in the wavelength range 300 nm - 800 nm of the ZnO thin films, AZO thin films and the bare Zeonor substrate. It is observed that, for all the ZnO and AZO films deposited at oxygen pressures above 3.33 Pa (25 mTorr), the transmission is high (85-95 %), featuring a sharp fundamental absorption edge and a well-developed pattern of multiple-beam interference fringes. This suggests that the films grown in these conditions have generally uniform thickness and sharp interfaces. The transmission of the films deposited at low oxygen pressures (0.13 Pa (1 mTorr) and 1.33 Pa (10 mTorr)) drops to 70-85 % with significantly less pronounced fringe patterns and more diffuse onset of the fundamental absorption edge. Several factors are found that likely contribute to these observations. Firstly, the AFM data show significantly increased rms surface roughness for these films (Fig.2) which will result in local thickness variations and increased diffuse reflective scattering. Gondoni *et al*. [48] have observed similar behavior for ZnO films deposited on soda-lime glass substrates in comparable conditions. Secondly, the progressive degradation of structural quality observed for these films (Fig. 3) will contribute to the disappearance of a sharp fundamental absorption edge and reduction in transmission. Thirdly, the significant defect-related increase in free carrier concentration observed for these films (see Fig.6 and the comments of Section 3.4) leads to increased visible and long-wavelength absorption. This is the expected behavior in transparent conductive oxides [49].

The low temperature PL spectra for the ZnO and AZO films grown at oxygen pressures of 0.13, 3.33 and 10 Pa are shown in Figure 5. This comprises the low pressure range of our study in which physical property changes have been noted in the previous sections. The PL behavior for the samples grown at pressures of 10 Pa and above remains similar [26] and need not be shown here. Figure 5 shows high intensity and spectrally broadened characteristic near band edge (NBE) emission in the UV region for all the films. The NBE emission is due to excitonic

recombinations. The NBE large spectral widths indicate significant inhomogeneous broadening which can be, at least partly, explained in terms of stress effects related to the changes of surface morphology and structural property discussed above for the samples grown at 0.13 and 3.33 Pa oxygen pressures. An additional strong deep level emission (DLE) in the 575 – 700 nm wavelength region is observed in the 10 Pa ZnO sample only. Many works have showed that this long wavelength emission in ZnO is associated with electronic bands formed by excess oxygen either as an interstitial (O_i) point defect [50] or a surface adsorbed species [51]. These interpretations are consistent with the observed DLE disappearance in the spectra of the 0.13 and 1.33 Pa samples. A possible explanation for the absence of the DLE emission in all AZO samples has been put forward previously [26]. Overall, the dominant broad NBE emission in these samples indicates that ZnO and AZO films grown at low oxygen pressures would be useful in UV and white light LED applications.

3.4 Electrical properties

Fig. 5 shows the electrical properties (resistivity, Hall mobility and carrier concentration) of the as-grown films, i.e. without post-processing annealing or activation treatments. All the electrical measurements were performed at room temperature and atmospheric pressures. For the ZnO films grown above 3.33 Pa (25 mTorr) oxygen pressure, the resistivity is ~ 10^3 - 10^5 Ω cm and the films are semi-insultating. The resistivity of the films dropped sharply to 10^{-2} - 10^{-3} Ω cm for the lower oxygen growth pressures of 0.13 Pa (1 mTorr) and 1.33 Pa (10 mTorr). This decrease in resistivity may be attributed to variations of the oxygen vacancy concentration. A decrease of the oxygen pressure is known to increase the number of oxygen vacancies, and, thus, the carrier concentration and conductivity in ZnO thin films [40,47,48]. As the oxygen pressure decreases, the Hall mobility peaks around 35 cm^2/V-s at 3.33 Pa (25 mTorr) and then decreases to ~ 2 cm^2/V-s at 0.13 Pa (1 mTorr). This behavior

correlates closely with the pressure-dependent morphological and crystalline changes observed previously. The Hall mobility variations can be explained in terms of pressure-dependent changes in both grain boundary and defect scattering [47]. The decrease of grain size with oxygen pressure (Table 1) leads to an increase in grain boundary scattering while defect scattering also increases due to the larger oxygen vacancy concentrations at low oxygen pressures. Carrier concentration (n-type) increases sharply from 10^{9} cm^{-3} to 10^{21} cm^{-3} as the oxygen pressure decreases from 10 Pa (75 mTorr) to 0.13 Pa (1 mTorr), which may be attributed to the increased number the oxygen vacancies at lower oxygen growth pressures [40,47,48]. The AZO films show generally improved electrical behavior in terms of resistivity compared to ZnO films, particularly at oxygen pressures greater than 10 Pa (75 mTorr). This is evidently due to the increased free electron concentration provided by the Al donor dopant. The resistivity decreases with oxygen pressure from a maximum value of ~ 10^{3} Ω cm at oxygen pressures of 10 Pa (75 mTorr) and above, to a minimum value around 10^{-3} - 10^{-4} Ω cm at the 0.13 Pa (1 mTorr) pressure. The Hall mobility peak value is 18 cm^{2}/V-s for an oxygen growth pressure of 5.33 Pa (40 mTorr) and drops to values of 1 - 5 cm^{2}/V-s at pressures of 3.33 Pa (25 mTorr) and below. The AZO films (n-type) carrier concentration increases sharply from 10^{15} cm^{-3} to 10^{21} cm^{-3} as the oxygen pressure decreases from 10 Pa (75 mTorr) to 0.13 Pa (1 mTorr). Due to the similarity of the oxygen pressure-dependent morphological and crystalline behaviors observed for ZnO and AZO, the arguments invoked above to explain the pressure-dependence of the ZnO films electrical properties can also be used for the AZO films.

4. Conclusions

The effects of oxygen growth pressure on surface morphology, structural, optical and electrical properties of as-grown ZnO and AZO thin films deposited on Zeonor polymer substrates by room temperature pulsed-laser deposition were studied. As the oxygen pressure decreases from 10 Pa (75 mTorr) to 0.13 Pa (1 mTorr), the following marked changes are observed. (i) The deposit surface morphology changes from nanocrystalline to a continuous film-like form and the surface rms roughness increases significantly from 5 nm to 65 nm, primarily due to the appearance of long and deep valley-shaped cracks. (ii) The degree of hydrophobicity of the samples decreases with a shift to hydrophilic behavior for the 0.13 Pa (1 mTorr) oxygen pressure samples. (iii) The orientation of the crystalline fraction of the deposit shifts from *c*-plane to *m*-plane for the ZnO and AZO materials. (iv) The average visible optical transmittance decreases significantly from ~ 95 % to ~ 65 %, while both the bandedge onset and the multiple-beam fringe patterns become quite diffuse due to increased scattering and film non-uniformity. The strong orange/red DLE emission in ZnO films was quenched. (v) The electrical properites are significantly improved overall, for example the resistivity of the ZnO films decreases from ~ 10^{5} Ω cm to 10^{-3} Ω cm while the carrier concentration increases from ~ 10^{9} - 10^{15} cm^{-3} to 10^{21} cm^{-3}.

Overall, the effect of oxygen pressure on the structure and properties of ZnO and AZO films has been demonstrated to be an important factor, potentially enabling researchers to control and tailor the properties of ZnO and AZO films on polymer substrates such as Zeonor. The combination of a low-water absorbing polymer substrate like Zeonor and an optically and electrically active ceramic layer like ZnO could help resolve the pervasive problem of gas permeation obviating diffusion-barrier layers. The findings of this work should be helpful for a range of applications in the field of flexible optoelectronics.

Acknowledgments

The authors acknowledge financial support from "INSPIRE (Integrated Nanoscience Platform for Ireland)" funded under the framework of the Irish Government's Programme for Research in Third Level Institutions Cycle 5, National Development Plan 2007-2013 with the assistance of the European Regional Development Fund, and thank Jennifer Gaughran for providing Zeonor sheets.

References

[1] S. Shahi, Flexible optoelectronics, Nat. Photonics 4 (2010) 506.

[2] K. Ellmer, Past achievements and future challenges in the development of optically transparent electrodes, Nat. Photonics 6 (2012) 809-817.

[3] T. Kamiya, H. Hosono, Material characteristics and applications of transparent amorphous oxide semiconductors, NPG Asia Mater. 2 (2010) 15-22.

[4] J.-Y. Kwon, D.-J. Lee, K.-B. Kim, Review paper: transparent amorphous oxide semiconductor thin film transistor, Electron. Mater. Lett. 7 (2011) 1-11.

[5] M. Weis, Transparent electrodes for flexible organic light-emitting diodes and displays, Display and Imaging 2 (2015) 49-68.

[6] J.F. Wager, B. Yeh, R.L. Hoffman, D.A. Keszler, An amorphous oxide semiconductor thin-film transistor route to oxide electronics, Curr. Opin. Solid St. M. 18 (2014) 53-61.

[7] C. Guillén, J. Herrero, TCO/metal/TCO structures for energy and flexible electronics, Thin Solid Films 520 (2011) 1-17.

[8] J.S. Park, W.-J. Maeng, H.-S. Kim, J.-S. Park, Review of recent developments in amorphous oxide semiconductor thin-film transistor devices, Thin Solid Films 520 (2012) 1679-1693.

[9] H. Hosono, Ionic amorphous oxide semiconductors: Material design, carrier transport, and device application, J. Non-Cryst. Solids 352 (2006) 851-858.

[10] T.C. Yeh, Q. Zhu, D.B. Buchholz, A.B. Martinson, R.H.P. Chang, T.O. Mason, Amorphous transparent conducting oxides in context: Work function survey, trends, and facile modification, Appl. Surf. Sci. 330 (2015) 405-410.

[11] H. Li, Y. Yu, M.B. Starr, Z. Li, X. Wang, Piezotronic-enhanced photoelectrochemical reactions in $Ni(OH)_2$-decorated ZnO photoanodes, J. Phys. Chem. Lett. 6 (2015) 3410-3416.

[12] Y. Hu, Y. Zhang, C. Xu, L. Lin, R.L. Snyder, Z.L. Wang, Self-powered system with wireless data transmission, Nano Lett. 11 (2011) 2572-2577.

[13] T. Rembert, C. Battaglia, A. Anders, A. Javey, Room temperature oxide deposition approach to fully transparent, all-oxide thin-film transistors, Adv. Mater. 27 (2015) 6090-6095.

[14] Y.-Y. Lin, C.-C. Hsu, M.-H. Tseng, J.-J. Shyue, F.-Y. Tsai, Stable and high-performance flexible ZnO thin-film transistors by atomic layer deposition, Appl. Mater. Interfaces 7 (2015) 22610-22617.

[15] F.B. Oruc, L.E. Aygun, I. Donmez, N. Biyikli, A.K. Okyay, H.Y. Yu, Low temperature atomic layer deposited ZnO photo thin film transistors, J. Vac. Sci. Technol. A 33 (2014) 01A105.

[16] J.-A. Jeong, H.-S. Shin, K -H. Choi, H.-K. Kim, Flexible Al-doped ZnO films grown on PET substrates using linear facing target sputtering for flexible OLEDs, J. Phys. D: Appl. Phys. 43 (2010) 465403.

[17] Y.-Y. Lin, Yi.-N. Chang, M.-H. Tseng, C.-C. Wang, F.-Y. Tsai, Air-stable flexible organic light-emitting diodes enabled by atomic layer deposition, Nanotechnology 26 (2015) 024005.

[18] S. Fernández, F.B. Naranjo, Optimization of aluminum-doped zinc oxide films deposited at low temperature by radio-frequency sputtering on flexible substrates for solar cell

applications, Sol. Energ. Mat. Sol. C 94 (2010) 157-163.

[19] M. Girtan, A. Vlad, R. Mallet, M.A. Bodea, J.D. Pedarnig, A. Stanculescu, D. Mardare, L. Leontie, S. Antohe, On the properties of aluminium doped zinc oxide thin films deposited on plastic substrates from ceramic targets, Appl. Surf. Sci. 274 (2013) 306-313.

[20] N. Zhou, D.B. Buchholz, G. Zhu, X. Yu, H. Li, A. Facchetti, T.J. Marks, R.P.H. Chang, Ultraflexible polymer solar cells using amorphous zinc-indium-tin oxide transparent electrodes, Adv. Mater. 26 (2014) 1098-1104.

[21] G.-J. Chang, S.-Y. Lin, J.-J. Wu, Room-temperature chemical integration of ZnO nanoarchitectures on plastic substrates for flexible dye-sensitized solar cells, Nanoscale 6 (2014) 1329-1334.

[22] M. Vähä-Nissi *et al*., Antibacterial and barrier properties of oriented polymer films with ZnO thin films applied with atomic layer deposition at low temperatures, Thin Solid Films 562 (2014) 331-337.

[23] A. Hatamie *et al*., Zinc oxide nanostructure-modified textile and its application to biosensing, photocatalysis, and as antibacterial material, Langmuir 31 (2015) 10913-10921.

[24] D.-Y. Cho, K.-H. Kim, T.-W. Kim, Y.-J. Noh, S.-I. Na, K.-B. Chung, H.-K. Kim, Transparent and flexible amorphous InZnAlO films grown by roll-to-roll sputtering for acidic buffer-free flexible organic solar cells, Org. Electron. 24 (2015) 227-233.

[25] H.R. Choi, S.K. Eswaran, S.M. Lee, Y.S. Cho, Enhanced fracture resistance of flexible ZnO:Al thin films in situ sputtered on bent polymer substrates, Appl. Mater. Interfaces 7 (2015) 17569-17572.

[26] S. Inguva, R.K. Vijayaraghavan, E. McGlynn, J.-P. Mosnier, Highly transparent and reproducible nanocrystalline ZnO and AZO thin films grown by room temperature pulsed-laser deposition on flexible Zeonor plastic substrates, Mater. Res. Express 2 (2015) 096401.

[27] L. Duan, X. Zhao, Y. Zhang, H. Shen, R. Liu, Fabrication of flexible Al-doped ZnO films

via sol-gel method, Mater. Lett. 162 (2016) 199-202.

[28] S.D. Cronin, K. Sabolsky, E.M. Sabolsky, K.A. Sierros, Dip pen nanolithography and transfer of ZnO patterns on platics for large-area flexible optoelectronic applications, Thin Solid Films 552 (2014) 50-55.

[29] Y.-H. Duan, Y. Fduan, P. Chen, Y. Tao, Y.-Q. Yang, Y. Zhao, High-performance flexible Ag nanowire electrode with low-temperature atomic-layer-deposition fabrication of conductive-bridging ZnO film, Nanoscale Res. Lett. 10 (2015) 90**.**

[30] M. Watanabe, L. Cui, R.H. Dauskardt, Atmospheric plasma deposition of transparent semiconducting ZnO films on plastics in ambient air, Org. Electron. 15 (2014) 775-784.

[31] N. Koteeswara Reddy, M. Devika, C.W. Tu, Vertically aligned ZnO nanorods on flexible substrates for multifunctional device applications: Easy and cost-effective route, Mater. Lett. 120 (2014) 62-64.

[32] X. Diez-Betriu, R. Jimenez-Rioboo, J. Sanchez-Marcos, E. Cespedes, A. Espinosa, A. de Andres, Amorphous-nanocrystalline Al doped ZnO transparent conducting thin films, J. Alloy Compd. 536S (2012) S445-S449.

[33] V. Zardetto, T.M. Brown, A. Reale, A.D. Carlo, Substrates for flexible electronics: A practical investigation on the electrical, film flexibility, optical, temperature, and solvent resistance properties, J. Polym. Sci. Pol. Phys. 49 (2011) 638-648.

[34] B. Visweswaran, P. Mandlik, S.H. Mohan, J.A. Silvernail, R. Ma, J.C. Sturm, S. Wagner, Diffusion of water into permeation barrier layers, J. Vac. Sci. Technol. A 33 (2015) 031513.

[35] W.R. Mateker, I.T. Sachs-Quintana, G.F. Burkhard, R. Cheacharoen, M.D. McGehee, Minimal long-term intrinsic degradation observed in a polymer solar cell illuminated in an oxygen-free environment, Chem. Mater. 27 (2015) 404-407.

[36] S.-J. Kang, C. Liu, Y.-Y. Noh, Vapor barrier films for flexible electronics, in: M. Caironi, Y.-Y. Noh (Eds.), Large area and Flexible Electronics, Wiley-VCH Velrlag GmbH & Co. KgaA., first ed., 2015, pp. 275-290.

[37] A. Miyake, T. Yamada, H. Makino, N. Yamamoto, T. Yamamoto, Effect of substrate temperature on structural, electrical and optical properties of Ga-doped ZnO films on cyclo olefin polymer substrate by ion plating deposition, Thin Solid Films 517 (2008) 1037-1041.

[38] M. Yamazaki, Industrialization and application development of cyclo-olefin polymer, J. Mol. Catal. A:Chem. 213 (2004) 81-87.

[39] Zeon Corporation, http://www.zeon.co.jp/, (accessed on 08.06.2016).

[40] H. Kim, Transparent Conducting Oxide Films, in: R. Eason (Eds.), Pulsed Laser Deposition of Thin Films: Applications-Led Growth of Functional Materials, Wiley, New Jersey, 2007, pp. 240-255.

[41] S.B. Kim, W.W. Lee, J. Yi, W.I. Park, J.-S. Kim, W.T. Nichols, Simple, large-scale patterning of hydrophobic ZnO nanorod arrays, ACS Appl. Mater. Interfaces 4 (2012) 3910-3915.

[42] D.P. Subedi, D.K. Madhup, A. Sharma, U.M. Joshi, A. Huczko, Study of the wettability of ZnO nanofilms, Int. Nano Lett. 1 (2011) 117-122.

[43] G. Socol *et al*., Pulsed laser deposition of transparent conductive oxide thin films on flexible substrates, Appl. Surf. Sci. 260 (2012) 42-46.

[44] S. Maniv, W.D. Westwood, E. Colombini, Pressure and angle of incidence effects in reactive planar magnetron sputtered ZnO layers, J. Vac. Sci. Technol. 20 (1982) 162-170.

[45] B.D. Cullity and S.R. Stock, Elements of X-ray Diffraction Third Edition, Prentice Hall, New Jersey (2001). [46] C. Guillen, J. Herrero, Structure, optical and electrical properties of Al:ZnO thin films deposited by DC sputtering at room temperature on glass and plastic substrates, Phys. Status Solidi A 206 (2009) 1531-1536.

[47] B.L. Zhu, X.Z. Zhao, S. Xu, F.H. Su, G.H. Li, X.G. Wu, J. Wu, R. Wu, J. Liu, Oxygen

pressure dependences of structure and properties of ZnO films deposited on amorphous glass substrates by pulsed laser deposition, Jpn. J. Appl. Phys. 47 (2008) 2225-2229.

[48] P. Gondoni, M. Ghidelli, F.D. Fonzo, M. Carminati, V. Russo, A.L. Bassi, C.S. Casari, Structure-dependent optical and electrical transport properties of nanostructured Al-doped ZnO, Nanotechnology 23 (2012) 365706.

[49] P.P. Edwards, A. Porch, M.O. Jones, D.V. Morgan, R.M. Perks, Basic Materials Physics of Transparent Conducting Oxides, Dalton Trans. (2004) 2995-3002; J.E. Medvedeva and A.J. Freeman, Combining High Conductivity with Complete Optical Transparency: A Band Structure Approach, Europhys. Lett. 69 (2005) 583-587.

[50] Cheol Hyoun Ahn , Young Yi Kim , Dong Chan Kim , Sanjay Kumar Mohanta , and Hyung Koun Cho, A comparative analysis of deep level emission in ZnO layers deposited by various methods, J. Appl. Phys. 105 (2009) 013502

[51] Amir R. Gheisi, Chris Neygandhi, Andreas K. Sternig, Esther Carrasco, Hubertus Marbach, Daniel Thomelec, Oliver Diwald, O2 adsorption dependent photoluminescence emission from metal oxide nanoparticles, Phys. Chem. Chem. Phys.16 (2014) 23922

Material	Oxygen pressure (Pa)	Film thickness (nm)	Orientation (*hkl*)	2θ (deg)	FWHM (deg)	Crystallite size (nm)	*c* (or *a*) parameter (nm)	Residual Stress (GPa)
ZnO	0.13	310	(100)	31.48	1.26	6.3	0.3282 (*a*)	-
	1.33	314	(002)	34.25	1.55	5.1	0.5237	-2.63
	3.33	321	(002)	33.87	1.71	4.7	0.5294	-7.58
	5.33	328	(002)	34.13	0.93	8.5	0.5256	-4.27
	10	340	(002)	34.34	0.44	19.7	0.5225	-1.48
	20	382	(002)	34.24	0.43	20.2	0.5240	-2.88
	40	422	(002)	34.26	0.41	21.4	0.5236	-2.53
AZO	0.13	181	(100)	31.50	1.11	7.2	0.3281 (*a*)	-
	1.33	188	(100)	31.48	1.11	7.2	0.3282 (*a*)	-
	3.33	201	(002)	34.15	2.59	3.1	0.5252	-3.92
	5.33	214	(002)	33.78	1.19	6.7	0.5308	-8.80
	10	263	(002)	34.45	0.49	17.1	0.5208	-0.09
	20	289	(002)	34.46	0.46	18.5	0.5207	-0.09
	40	415	(002)	34.52	0.64	12.8	0.5198	0.78

Table 1. Oxygen pressures used for the room temperature PLD of ZnO and AZO films on Zeonor substrates. The resulting films thickness, 2θ angular position and FWHM of the (002) or (100) XRD Bragg reflections, crystallite size, *c* (or *a*) -axis length and in-plane residual stress are given for the *c*-axis oriented films (estimated using bi-axial strain model of ref. [44]).

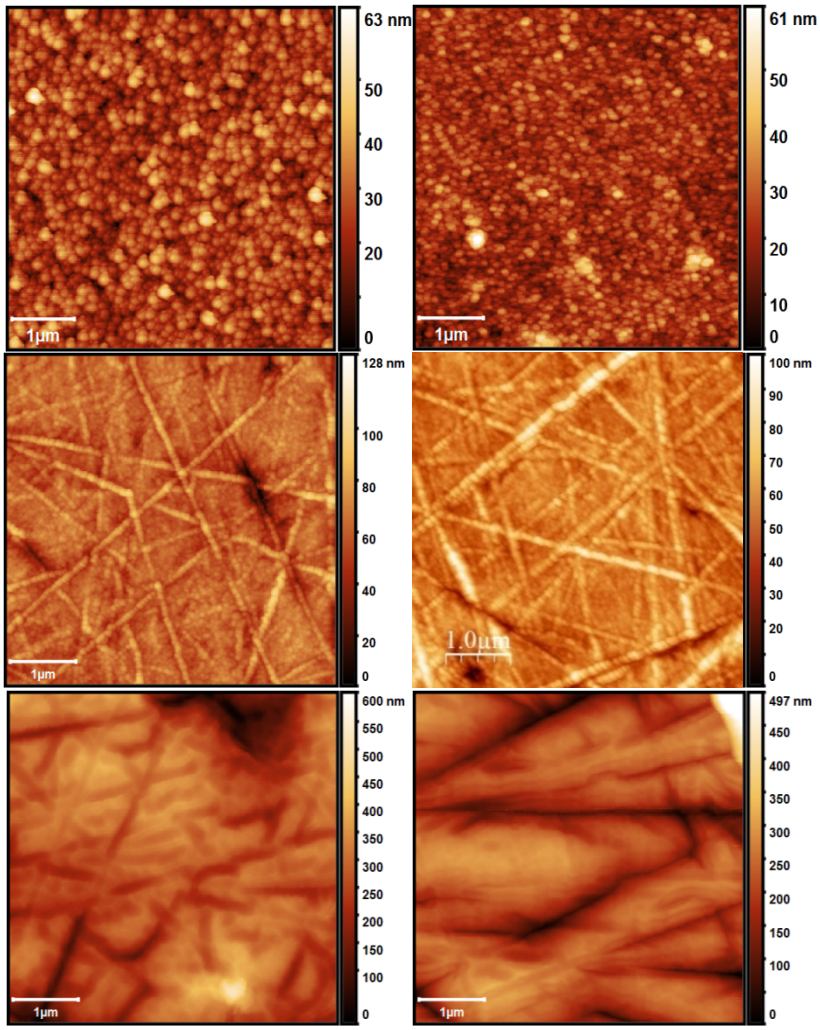

Figure 1. AFM images showing the surface morphology of ZnO (left-hand column) and AZO (right-hand column) thin films grown by room temperature PLD on Zeonor substrates in ambient oxygen pressures of 10 Pa (top panels), 3.33 Pa (middle panels) and 0.13 Pa (bottom panels).

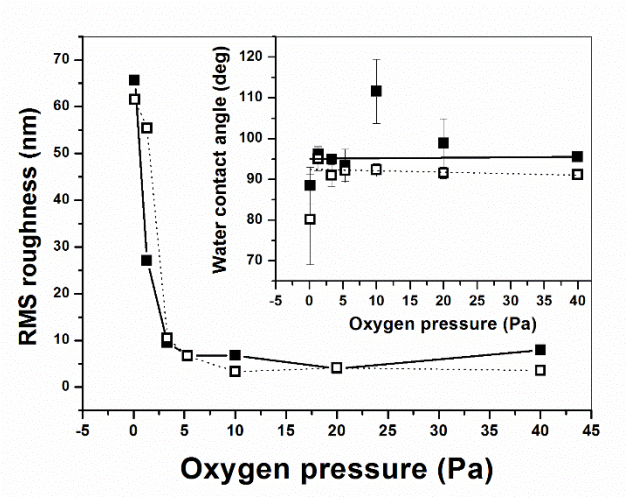

Figure 2. Root-mean square (rms) surface roughness and water contact angle (inset) for ZnO (closed symbols) and AZO (open symbols) thin films grown by room temperature PLD on Zeonor substrates as a function of oxygen growth pressure.

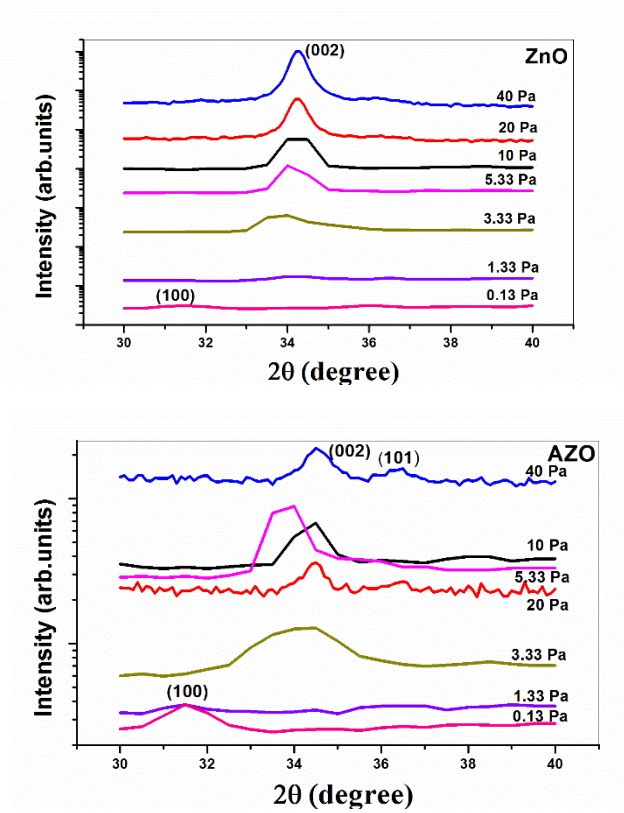

Figure 3. 2θ-ω XRD scans for ZnO and AZO thin films grown by room temperature PLD on Zeonor substrates in oxygen pressures between 0.13 Pa and 40 Pa.

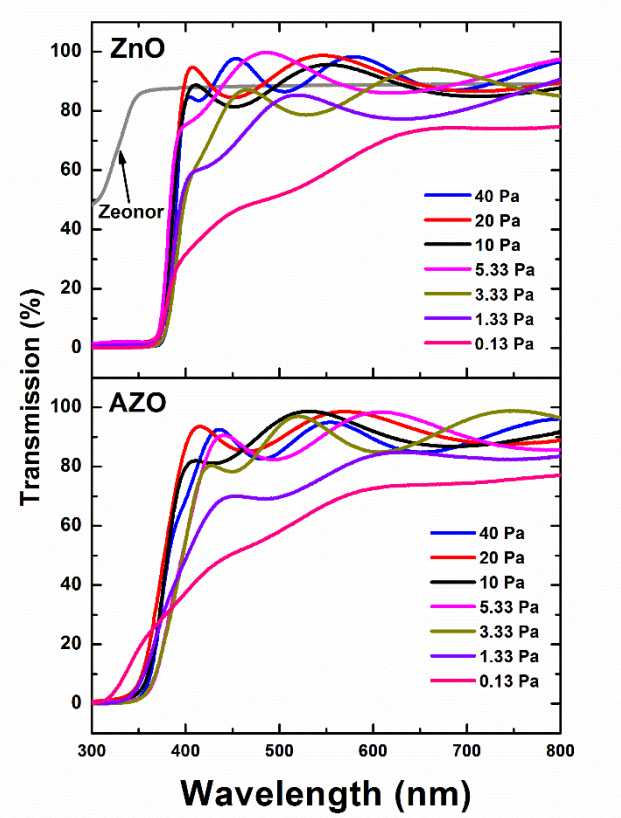

Figure 4. Optical transmission spectra in the 300 nm - 800 nm wavelength range for ZnO and AZO thin films grown by room temperature PLD on Zeonor substrates at oxygen pressures between 0.13 Pa and 40 Pa.

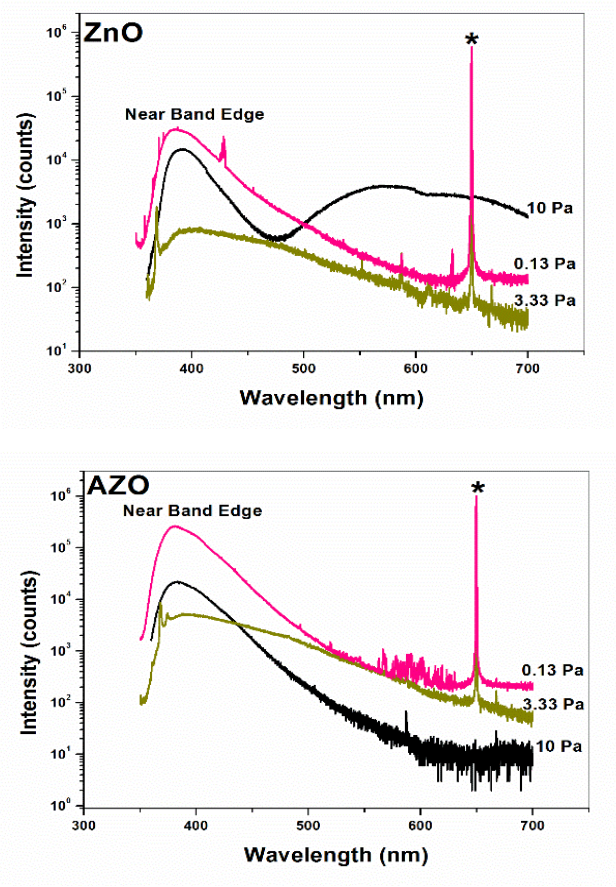

Figure 5. Low-temperature (13 K) PL spectra of the ZnO and AZO thin films grown by room temperature PLD on Zeonor substrates at oxygen pressures 0.13, 3.33 and 10 Pa. The feature marked '*' is scattered 325 nm excitation laser light diffracted in second order. The sharp line features in the NBE region of ZnO and AZO are interlopers originating in the HeCd gas discharge.

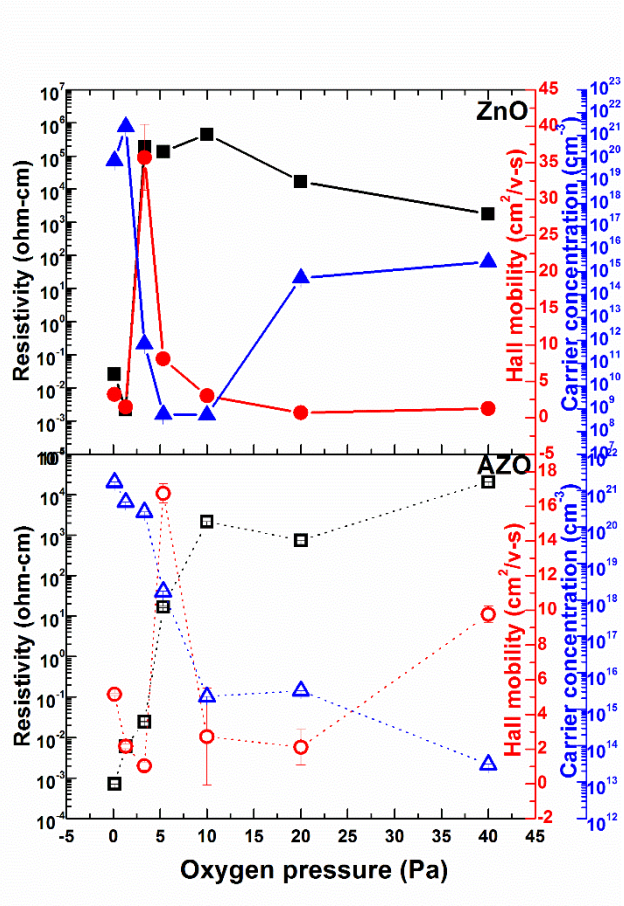

Figure 6. Resistivity (squares), Hall mobility (circles) and carrier concentration (triangles) of ZnO and AZO thin films grown by room temperature PLD on Zeonor substrates as a function of oxygen growth pressure.